Article

SOURCE
DATA

TRANSPARENT
PROCESS

EMBO
reports

PARIS undergoes liquid–liquid phase separation and poly(ADP-ribose)-mediated solidification

Hojin Kang[1,2,3,4,†], Soojeong Park[1,†], Areum Jo[1,2,3] iD, Xiaobo Mao[2,3] iD, Manoj Kumar[2,3], Chi-Hu Park[5] iD, Jee-Yin Ahn[4,6], Yunjong Lee[1,6] iD, Jeong-Yun Choi[1,6], Yun-Song Lee[1,6] iD, Valina L Dawson[2,3,7,8], Ted M Dawson[2,3,8,9] iD, Tae-In Kam[2,3,10,*] iD & Joo-Ho Shin[1,2,3,4,6,**] iD

Abstract

ZNF746 was identified as parkin-interacting substrate (PARIS). Investigating its pathophysiological properties, we find that PARIS undergoes liquid–liquid phase separation (LLPS) and amorphous solid formation. The N-terminal low complexity domain 1 (LCD1) of PARIS is required for LLPS, whereas the C-terminal prion-like domain (PrLD) drives the transition from liquid to solid phase. In addition, we observe that poly(ADP-ribose) (PAR) strongly binds to the C-terminus of PARIS near the PrLD, accelerating its LLPS and solidification. *N*-Methyl-*N*′-nitro-*N*-nitrosoguanidine (MNNG)-induced PAR formation leads to PARIS oligomerization in human iPSC-derived dopaminergic neurons that is prevented by the PARP inhibitor, ABT-888. Furthermore, SDS-resistant PARIS species are observed in the substantia nigra (SN) of aged mice overexpressing wild-type PARIS, but not with a PAR binding-deficient PARIS mutant. PARIS solidification is also found in the SN of mice injected with preformed fibrils of α-synuclein (α-syn PFF) and adult mice with a conditional knockout (KO) of parkin, but not if α-syn PFF is injected into mice deficient for PARP1. Herein, we demonstrate that PARIS undergoes LLPS and PAR-mediated solidification in models of Parkinson's disease.

Introduction

ZNF746 (parkin-interacting substrate, PARIS) is a parkin substrate and transcriptional regulator of peroxisome proliferator-activated receptor gamma coactivator 1-alpha (PGC-1α), contributing to dopaminergic neuronal death in Parkinson's disease (PD) (Shin *et al*, 2011). The inactivation of parkin leads to mitochondrial dysregulation by PARIS accumulation and PGC-1α suppression (Stevens *et al*, 2015). Our studies have also demonstrated that PARIS downregulates the production of ribosomal RNA and transketolase through the occupation of their promoters (Kang & Shin, 2015; Kim *et al*, 2017; Kang *et al*, 2018).

In neurodegenerative diseases, such as amyotrophic lateral sclerosis (ALS), Huntington's disease (HD), Alzheimer's disease (AD), and PD, there is evidence that disease-causing proteins are intrinsically disordered and prone to undergo liquid–liquid phase separation (LLPS). For instance, the RNA-binding protein FUS/TLS (FUS) and TAR DNA-binding protein 43 (TDP-43) in ALS (Patel *et al*, 2015; McGurk *et al*, 2018), huntingtin (HTT) in HD (Peskett *et al*, 2018), Tau in AD (Wegmann *et al*, 2018), and α-synuclein in PD (Ray *et al*, 2020) have intrinsically disordered regions (IDRs) and low complexity domains (LCDs) that enable LLPS. It is well known that proteins with IDRs and LCDs, which lack fixed three-dimensional structure, tend to transition to a liquid phase and aggregate (Shin & Brangwynne, 2017; Baradaran-Heravi *et al*, 2020). A protein with an IDR can undergo homogenous self-assembly into liquid droplets or a gel or solid state (Alberti & Dormann, 2019). The LCD is a type of IDR made up of only a few different types of amino acids. Interestingly, prion-like domain (PrLD) often exists in DNA- or RNA-binding proteins (Harrison & Shorter, 2017; McAlary *et al*, 2019) and enables their ability to undergo phase separation.

1 Department of Pharmacology, Sungkyunkwan University School of Medicine, Suwon, South Korea
2 Neuroregeneration and Stem Cell Programs, Institute for Cell Engineering, Johns Hopkins University School of Medicine, Baltimore, MD, USA
3 Department of Neurology, Johns Hopkins University School of Medicine, Baltimore, MD, USA
4 Single Cell Network Research Center, Sungkyunkwan University School of Medicine, Suwon, South Korea
5 Neurodegeneration Research Institute, YEP Bio Co., Ltd., Anyang, South Korea
6 Samsung Biomedical Research Institute, Samsung Medical Center, Seoul, South Korea
7 Department of Physiology, Johns Hopkins University School of Medicine, Baltimore, MD, USA
8 Solomon H. Snyder Department of Neuroscience, Johns Hopkins University School of Medicine, Baltimore, MD, USA
9 Department of Pharmacology and Molecular Sciences, Johns Hopkins University School of Medicine, Baltimore, MD, USA
10 Department of Brain and Cognitive Sciences, Korea Advanced Institute of Science and Technology, Daejeon, South Korea
   *Corresponding author. Tel: +1 410 502 4400; E-mail: tkam1@jhmi.edu
   **Corresponding author. Tel: +82 31 2399 6192; E-mail: jshin24@skku.edu
   †These authors contributed equally to this work

Since protein aggregation is a hallmark of neurodegenerative diseases, dysregulation of phase separation has emerged as a potential pathological mechanism (Franzmann & Alberti, 2019).

Poly(ADP-ribose) (PAR) is a polymer consisting of ADP-ribose units that regulates diverse cellular functions through covalent conjugation of PAR to substrate proteins (PARylation) or PAR binding to specific sites. Recently, PAR has been shown to act as a molecular seed for the condensation of proteins that contain IDRs (Altmeyer *et al*, 2015). DNA damage or physiological stress can lead to an increase in PAR levels where PAR promotes liquid demixing of IDR-containing proteins, such as FUS, Ewing sarcoma protein (EWS), and TATA box-binding protein-associated factor (TAF-15) and TDP-43 (Altmeyer *et al*, 2015; Patel *et al*, 2015; McGurk *et al*, 2018). In PD, pathologic α-synuclein and aminoacyl tRNA synthase complex-interacting multifunctional protein 2 (AIMP2) can activate PAR polymerase 1 (PARP1), which in turn produces PAR (Lee *et al*, 2013; Kam *et al*, 2018), contributing to dopaminergic neuronal death (Dawson & Dawson, 2017; Berger *et al*, 2018; Kam *et al*, 2018). In this study, we show that the PD-associated transcriptional repressor PARIS possesses LCDs, and PARIS undergoes a liquid-to-solid phase transition that is enhanced by PAR. Moreover, we demonstrate PAR-mediated PARIS solidification in the substantia nigra (SN) of PD animal models including aged mice overexpressing wild-type PARIS, preformed fibrils of α-synuclein (α-syn PFF)-injected mice, and adult conditional parkin knockout (KO) mice.

Results

PARIS undergoes dynamic phase separation *in vitro*

Pfam domain prediction and Predictor of Natural Disordered Regions (PONDR) reveals that PARIS has five LCDs and IDRs throughout the PARIS protein sequence (Fig 1A). To determine whether these IDRs and LCDs in PARIS protein could potentially facilitate phase separation (Toretsky & Wright, 2014), we performed *in vitro* phase separation assay with Glutathione S-transferase (GST)-tagged PARIS (GST-PARIS) recombinant protein at different concentrations (Fig 1B, Appendix Fig S1A). PARIS spontaneously started to form liquid droplets at 10 μM concentration under physiological salt levels (150 mM NaCl). Higher salt concentration (500 mM NaCl) accelerated LLPS of PARIS. *In vitro* PARIS formed an amorphous-shaped solid at 50 μM, indicating that PARIS underwent LLPS and solid-state phase transition with increasing concentration (Fig 1B). With a crowding reagent, 10% polyethylene glycol (PEG), PARIS aggregated at physiological salt concentrations that was diminished by disrupting hydrophobic interactions with 10% 1,6-hexanediol (Fig 1C). PARIS (20 μM) droplets can undergo fusion and fission confirming that PARIS droplets have liquid-like properties (Fig 1D, Appendix Fig S1B, Movies EV1 and EV2). PARIS exhibited wetting properties since PARIS droplets adhered to the surface of the glass slide at 3 min and this wetting increased at 5 min (Fig 1E).

PARIS transitions from liquid droplets to amorphous aggregates

Fluorescence recovery after photobleaching (FRAP) was utilized to examine the PARIS liquid droplet versus the PARIS aggregates generated with 10 and 50 μM PARIS, respectively (Fig 2A, Movies EV3 and EV4). The liquid droplet of PARIS at 10 μM concentration showed rapid ($t_{1/2}$ = 4.424 s) and complete fluorescence recovery. On the other hand, the mobility of PARIS aggregates at 50 μM concentration was substantially decreased ($t_{1/2}$ = 9.897 s) and showed only 25% fluorescence recovery (Fig 2B and C). We monitored the morphology of PARIS at various time points by transmission electron microscopy (TEM). 10 μM PARIS droplets start to form seed-like oligomers on day 3. Liquid to solid transition was observed on day 7 and PARIS converted into amorphous aggregates on day 14. The amorphous aggregation of PARIS continued to day 21 (Fig 2D). A higher concentration of PARIS (50 μM) actively produced amorphous aggregates (Appendix Fig S2A and B). Moreover, after 14 days of incubation, the aggregates of PARIS (10 μM) generated completely lost the biophysical properties of the liquid stage, as evidenced by only 25% fluorescence recovery (Appendix Fig S2B). The integrity of both GST-tagged and GST-cleaved PARIS recombinant proteins was confirmed through Coomassie blue staining (Appendix Fig S2C).

Next, we applied circular dichroism (CD) spectrometry to investigate the secondary structure of the solid assembly of PARIS at various time points. The CD data show that PARIS has an β-sheet-rich structure on day 0, and the self-oligomeric structure appeared on day 3. From day 7, PARIS failed to show a typical secondary structure, demonstrating the formation of the amorphic aggregate (Appendix Fig S3A). We observed a characteristic minimum of β-sheet structure at 215 nm in the CD spectrum of PARIS at day 0. After 3 days of PARIS protein incubation, we observed a change in the CD spectrum in the far UV, indicating a loss of β-sheet secondary structure in PARIS (Appendix Fig S3A).

In addition, the slopes of the CD spectrum between 230 and 240 nm (so-called the 230–240 nm slope method) strongly correlate with the helix contents, including α-helix and 3_{10}-helix of protein (Ahel *et al*, 2008; Wei *et al*, 2014). In our results, the CD spectrum$_{230–240\ nm}$ slopes of PARIS decreased as the protein aged (Appendix Fig S3A). This suggests that protein aging shifts the secondary structure of PARIS towards an amorphous structure. To test whether PARIS forms amyloid-like aggregates, we applied thioflavin T staining. PARIS did not form amyloid fibrils as assessed by thioflavin T staining during the 14 days of incubation (Appendix Fig S3B). The results taken together suggest that PARIS droplets can transition to amorphous aggregates according to the protein concentration and the length of incubation.

Identification of LCD requirement for PARIS LLPS

To further characterize PARIS's ability to undergo LLPS and liquid to solid transition, the amino acid composition of the PARIS LCD was examined. PARIS harbors clusters containing polar and charged amino acids (glycine (G), serine (S), glutamine (Q), proline (P), glutamic acid (E), lysine (K), and arginine (R)) and prion-like LCD, which is known to drive phase transition (Nott *et al*, 2015) (Fig 3A, top panel). The glycine-rich region (amino acid 476–516, https://www.uniprot.org/uniprot/Q6NUN9) containing LCD4 (amino acid 475–507, Fig 1A) was predicted as a PrLD by PLAAC (amino acid 486–499) (http://plaac.wi.mit.edu/) (Fig 3A, bottom panel). To identify the crucial region for PARIS LLPS, LCD-deficient PARIS mutants (PARIS ΔLCDs) were generated and used for the LLPS
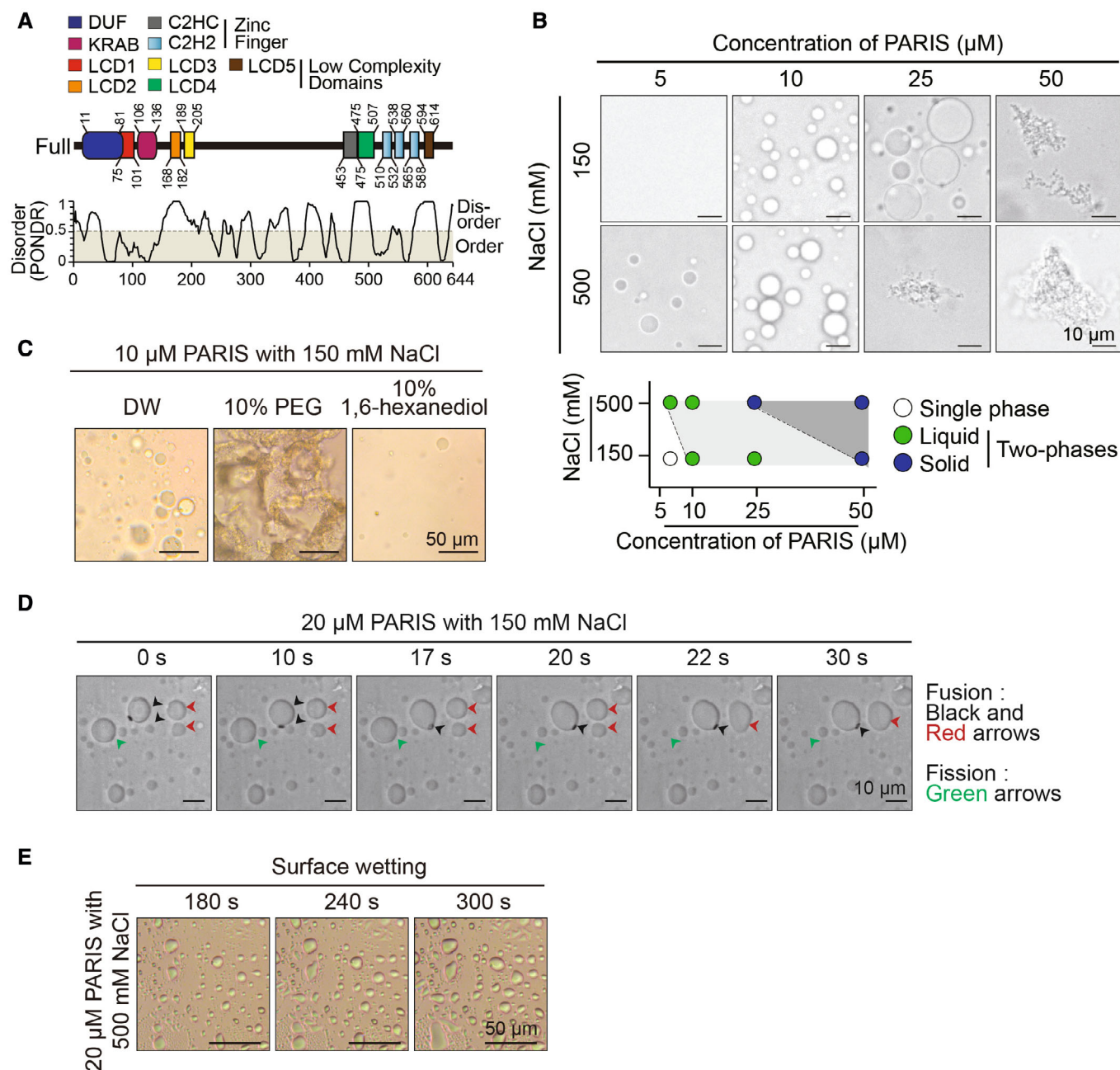
Figure 1. PARIS undergoes liquid–liquid phase separation.

A Full-length PARIS sequence analysis and disorder prediction by PONDR. PARIS contains DUF, KRAB, zinc fingers, and 5 low complexity domains (LCDs). In the bottom panel, 10 highly disordered regions were peaked.

B Phase separation of recombinant GST-tagged PARIS protein at 5, 10, 25, and 50 μM protein concentration with 150 mM or 500 mM NaCl (top panel). Diagram shows the state of PARIS at the indicated condition (bottom panel).

C Phase separation assay with GST-tagged PARIS (10 μM, 150 mM NaCl) treated with 10% polyethylene glycol (PEG) or 1,6-hexanediol.

D Fusion and fission dynamics of GST-tagged PARIS liquid droplets (20 μM, 150 mM NaCl).

E Surface wetting of 20 μM GST-tagged PARIS with 500 mM NaCl.

Source data are available online for this figure.

assays. PARIS ΔLCD1 failed to undergo LLPS at 10 μM and formed liquid droplets at 50 μM, indicating that the formation of the liquid phase was prior to the solid assembly of PARIS (Fig 3B). PARIS ΔLCD4 formed liquid droplets but not solid aggregates (Fig 3B). PARIS ΔLCD2, ΔLCD3, and ΔLCD5 had no appreciable effect on liquid droplets or the formation of aggregates (Fig 3B). These data
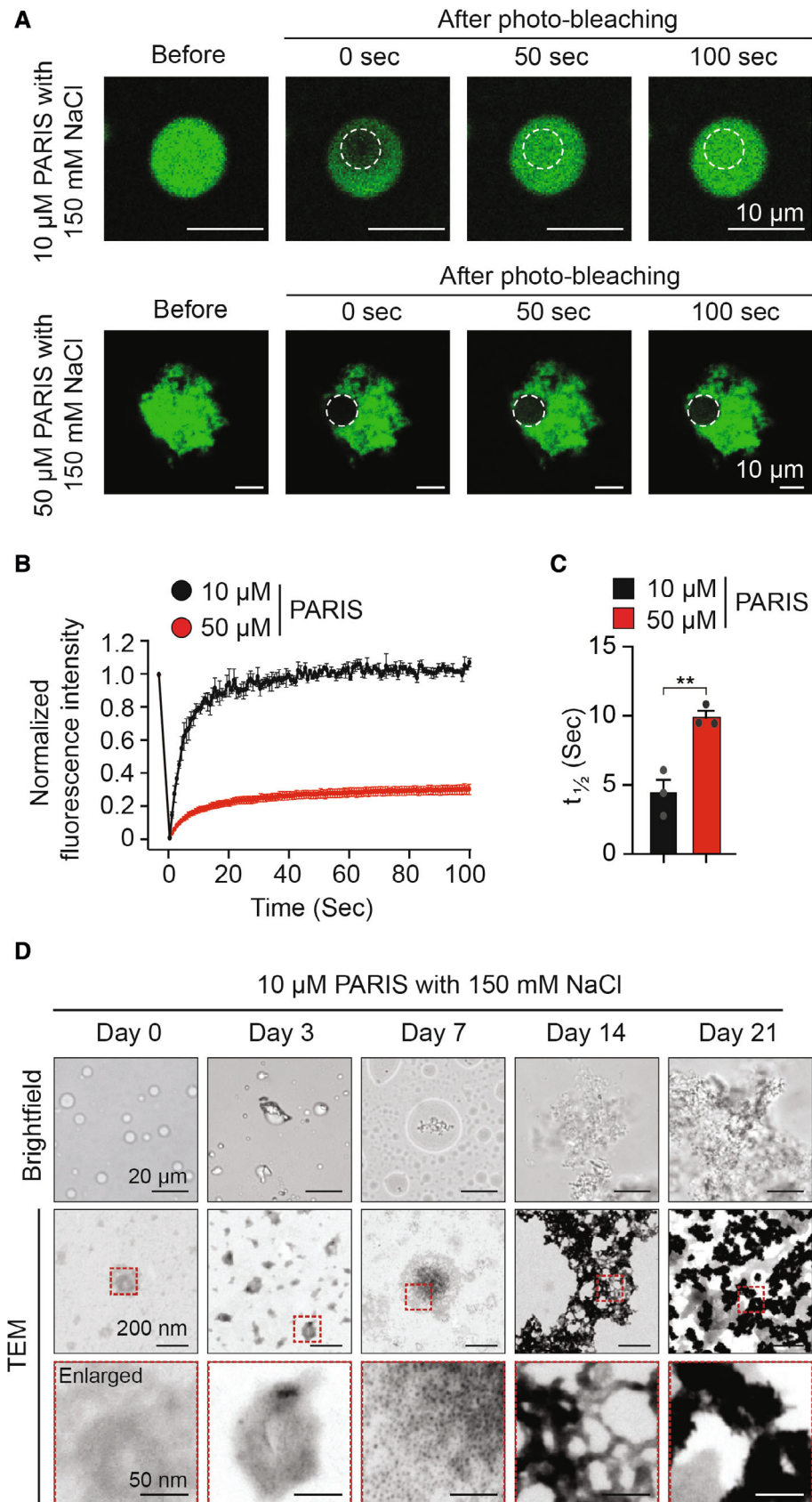
Figure 2.

Figure 2.   Protein aging of PARIS converts liquid droplets to amorphous aggregates.

A   Representative image of fluorescence recovery after photobleaching (FRAP) analysis with 10 or 50 μM GFP-tagged PARIS recombinant protein.
B   Normalized fluorescence intensity of panel (A), $n = 3$ per independent experiment.
C   Calculated $t_{1/2}$ value through fluorescence recovery of (A), $n = 3$ per group. Statistical significance was determined by Student's *t*-test. Data are expressed as mean ± SEM of three biological replicates. **$P < 0.01$.
D   Transmission electron microscope (TEM) image of GST-tagged PARIS protein (10 μM, 150 mM NaCl) at indicated time point. Red rectangles were enlarged in the bottom panel.

Source data are available online for this figure.

suggest that LCD1 is responsible for LLPS, and LCD4 is involved in the liquid to solid transition of PARIS (Fig 3B).

Since LCD4 appears to be important for PARIS aggregation, we hypothesized that the PrLD of LCD4 could affect the formation of solid PARIS. PrLD-deficient PARIS (ΔPrLD) was examined for LLPS and demonstrated that both PARIS WT and PARIS ΔPrLD recombinant protein (10 μM) formed liquid droplets. PARIS ΔPrLD formed smaller droplets compared to PARIS WT. At higher concentrations (50 μM) of PARIS, PARIS WT aggregated, whereas PARIS ΔPrLD produced bigger droplets rather than solid species (Fig 3C). Moreover, PARIS double ΔLCD1; ΔPrLD mutants failed to form liquid droplets and solid aggregates (Fig 3C). To confirm the requirement of LCD1 for PARIS LLPS, we constructed GFP-tagged PARIS truncation mutants (TMs). These fragments were co-transfected into SH-SY5Y cells with Flag-tagged full-length PARIS and were subjected to immunoprecipitation. GFP-tagged PARIS TM#1 containing LCD1 was pulled down with full-length Flag-tagged PARIS, suggesting that the self-binding of PARIS is dependent on the LCD1-containing N-terminus of PARIS (Appendix Fig S4A). Synthetic LCD1 peptides exhibited LLPS confirming that LCD1 is a core self-binding region for PARIS (Appendix Fig S4B). Taken together, these findings indicate that LCD1 is critical for PARIS LLPS, and the PrLD is required for the liquid to solid transition of PARIS.

To investigate the possibility of PARIS LLPS *in vivo*, we transiently transfected SH-SY5Y cells with either GFP-tagged PARIS LCD1 or GFP-PARIS WT and monitored their cellular dynamics at 12 and 24 h post-transfection. We observed the liquid droplets of GFP-PARIS LCD1 and confirmed their liquidity by monitoring droplet fusion and dynamics (Appendix Fig S4C). Interestingly, we found the formation of droplets of PARIS WT in the nucleus at 24 h post-transfection, which was not detected at 12 h post-transfection (Appendix Fig S4D).

PAR binds to the zinc finger domain of PARIS

Since PAR is considered an LLPS modulator in neurodegenerative diseases (Leung, 2020), we tested whether PAR interacts with PARIS and affects PARIS LLPS. A PAR overlay assay showed that PAR bound to GST-Histone H3 (positive control) and GST-PARIS but not to GST (negative control) and GST-ZNF398 (PARIS homolog, negative control) (Fig 4A). PARIS showed significantly higher PAR-binding than histone H3.

Next, we investigated PARIS LLPS in the presence of PAR. The addition of 10 nM PAR triggered the liquid demixing of PARIS at 5 μM (Fig 4B). Similarly, 10 nM PAR accelerated the solid assembly of PARIS (25 μM). At concentrations of 50 μM PARIS, robust solid transitions were observed with or without PAR (Fig 4B). To test the specificity of the liquid–solid transition of PARIS (25 μM) by PAR, we applied highly negatively charged nucleic acids, either 10 nM random hexamer DNA or 10 nM sonicated HeLa cell RNA, as control, to the process of PARIS LLPS (Fig 4C). Random hexamer DNA or sonicated HeLa cell RNA only showed small-sized liquid droplets and solid particles in contrast to the large liquid droplets induced by PAR (Fig 4C). These results suggest that PAR specifically enhances PARIS LLPS.

To identify the PAR-binding region of PARIS, the PARIS TMs (see Appendix Fig S4) were subject to a PAR overlay assay (Appendix Fig S5A). TM#7 containing the C2H2 zinc fingers appeared to be a PAR-binding region in PARIS (Appendix Fig S5A). To generate a PAR binding-deficient mutant (PDM) of PARIS, an *in silico* search for consensus lysine and arginine (KR) PAR-binding sites (Krietsch *et al*, 2013) in TM#7 identified three plausible PAR-binding motifs (PBMs) (Appendix Fig S5B). PBM and its interaction with PAR are likely due to electrostatic interactions between the positively charged amino acids present in the PBM consensus ([HKR]-X-X-[AIQVY]-[KR]-[KR]-[AILV]-[FILPV]) and the negatively charged PAR chains (Gagne *et al*, 2008). Plausible PAR-binding site #2 (573-KSFIRKDH-580) and #3 (578-KDHLRKHQ-585) of PARIS is comparable to the PBM consensus sequence, whereas PAR-binding site #1 (536-RPFPCTECEKRFTER SKLIDHYRTH-560) is similar to the consensus sequence ([K/R]-X-X-C-X-[F/Y]-G-X-X-C-X-[K/R]-[K/R]-X-X-X-X-H-X-X-X-[F/Y]-X-H) identified in a Cys2-His2 type zinc finger motif of two DNA damage responsive proteins APLF (aprataxin and PNK-like factor) and CHFR (checkpoint with forkhead and ring finger domains) (Appendix Fig S5B) (Ahel *et al*, 2008). PDMs containing single, double, or triple point mutations were generated and followed by an *in vitro* PAR overlay assay. The single and double PDMs showed weaker PAR-binding compared to WT, whereas the triple PDM completely lost its PAR-binding (Appendix Fig S5B). To confirm if non-denatured PARIS can bind to PAR, recombinant GST-tagged PARIS WT, TM#7, deletion #7 (Δ#7), and triple PDM proteins were used in dot blot analysis for PAR binding (Fig 4D). GST-PARIS WT and GST-PARIS TM#7 showed an interaction with PAR, while GST-PARIS Δ#7 and GST-PARIS triple PDM failed to bind to PAR (Fig 4D). In the absence of PAR, GST-PARIS WT, and GST-PARIS triple PDM undergo LLPS (Fig 4E). In the presence of PAR, PARIS WT undergoes liquid to solid transition while the PARIS triple PDM only undergoes LLPS regardless of PAR (Fig 4E).

To confirm the binding of PAR to PARIS in cells, SH-SY5Y cells were transfected with Flag-tagged PARIS WT and triple PDM, followed by MNNG and treatment with the PARP inhibitor, PJ34. Immunoprecipitated WT and triple PDM PARIS were dot-blotted with a PAR antibody. PAR co-immunoprecipitated with PARIS WT in MNNG-treated cells, which was significantly
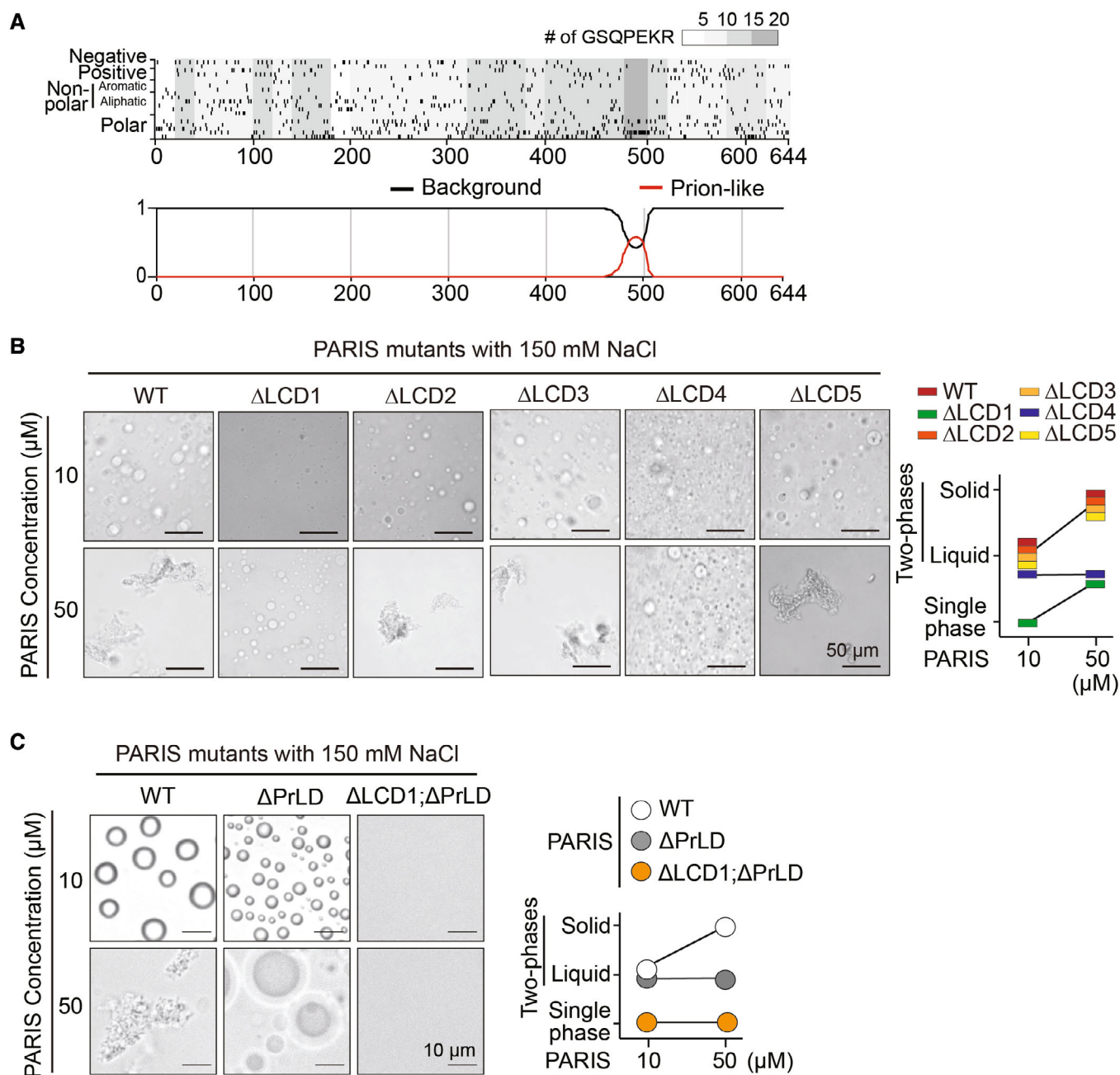
Figure 3. Low complexity region is required for phase separation of PARIS.

A Distribution of amino acids in the sequence of PARIS. Amino acids were classified as negatively or positively charged, nonpolar, and with polar properties. The number of glycine (G), serine (S), glutamine (Q), proline (P), glutamic acid (E), lysine (K), and arginine (R) residues are counted and color-corded (Top panel). Prion-like domain prediction of PARIS by PLAAC analysis (bottom panel).

B Phase separation assay with low complexity domain (LCD)-deficient GST-tagged PARIS (ΔLCD). Wild-type and deletion mutant GST-tagged PARIS proteins (10 and 50 μM) were incubated in 150 mM NaCl. The right panel indicates the phase diagram.

C The left panel shows LLPS of GST-tagged PARIS WT, prion-like domain (PrLD)-deficient mutant (ΔPrLD), and double deletion mutant (ΔLCD1;ΔPrLD). The right diagram indicates a phase of protein in a given condition.

Source data are available online for this figure.

diminished by PJ-34 (Appendix Fig S5C). However, triple PDM did not show PAR binding (Appendix Fig S5C). In addition, Flag-tagged PARIS WT and triple PDM were transiently transfected into PARP1 WT or KO cell lines. Immunoprecipitated PARIS WT and triple PDM were separated through SDS–PAGE and immuno-blotted with the PAR antibody. The covalent attachment of PAR

A

B

PARIS (μM) with 150 mM NaCl

C

PARIS (25 μM) with 150 mM NaCl

D

E

25 μM PARIS
with 150 mM NaCl
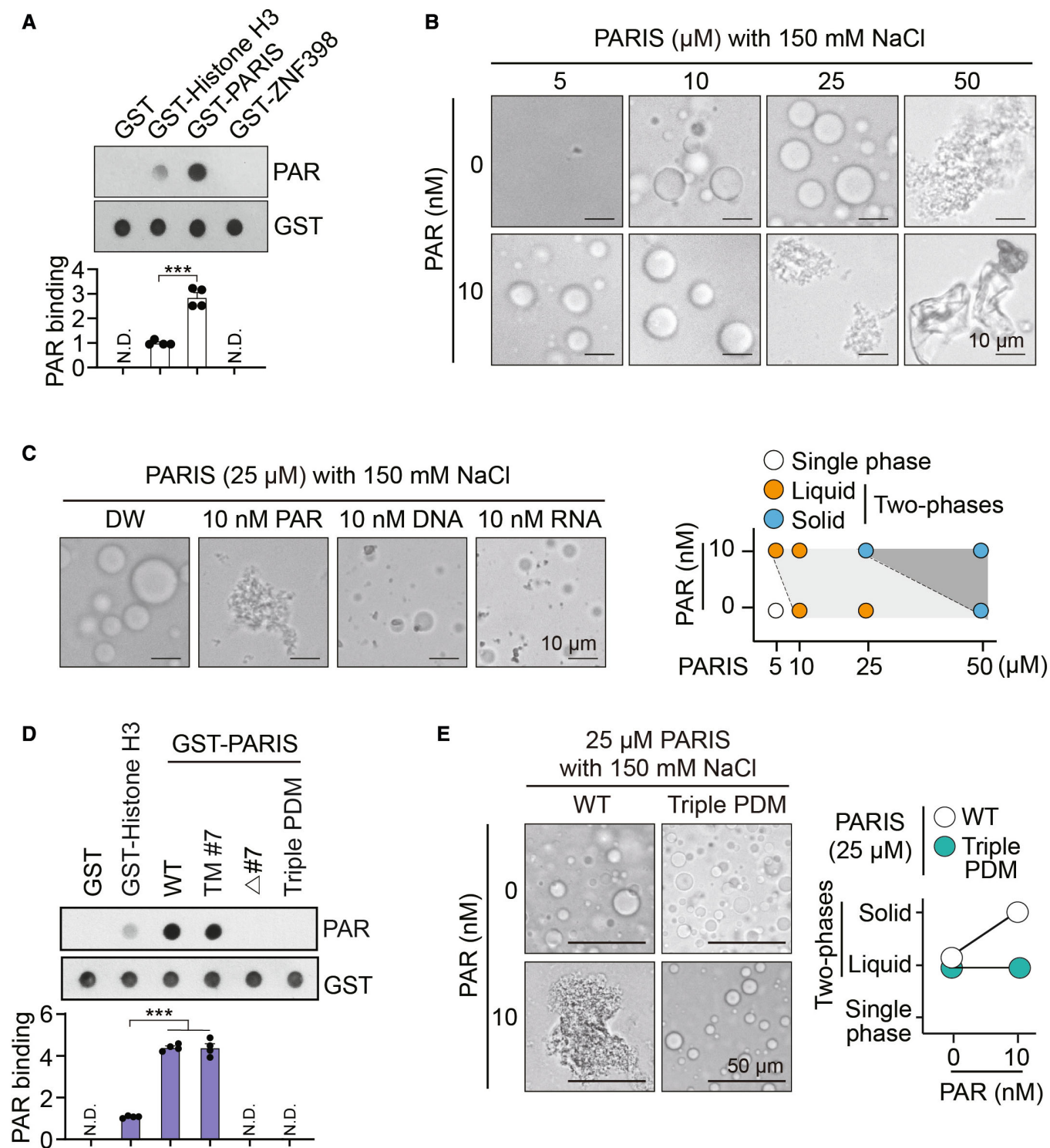
Figure 4.

with PARIS WT was not detected in PARP1 WT cells, indicating that PARIS is not PARylated (Appendix Fig S5D). PARylated PARP1 was detected in the immunoprecipitates of both Flag-PARIS WT and triple PDM in PARP1 WT cells but not in PARP1 KO cells (Appendix Fig S5D).

PAR enhances the amorphous aggregation of PARIS

To monitor the progression of PARIS aggregation in the presence of PAR, an *in vitro* aggregation assay, followed by SDS–PAGE, was performed. PARIS (10 μM) was incubated in the presence of 10 nM

Figure 4. PAR promotes phase separation of PARIS.

A PAR overlay assay with GST, GST-Histone H3 (positive control), GST-PARIS WT, and GST-ZNF398 (negative control).

B Dynamic phase separation of 5, 10, 25, and 50 μM GST-PARIS in the presence of 10 nM PAR. The status of PARIS phase is illustrated at the bottom.

C Phase separation of PARIS (25 μM) in the presence of 10 nM PAR, DNA, or RNA. DNA, random hexamer; RNA, sonicated RNA of HeLa cells.

D PAR overlay assay of recombinant GST-PARIS WT and mutant proteins (TM#7, Truncate #7; Δ#7, #7 deletion; triple PDM, triple PAR binding-deficient mutant).

E Phase separation assay with GST-PARIS WT and triple PDM with or without 10 nM PAR. The phase diagram is on the right side.

Data information: For (A) and (D), statistical significance was determined by one-way ANOVA test with Tukey *post-hoc* analysis. Data are expressed as mean ± SEM of four technical replicates. ***$P < 0.001$.

Source data are available online for this figure.

PAR for 12 days (Fig 5A). High molecular weight immunoreactivity of PARIS that was SDS resistant was detected after treatment with 10 nM PAR on the 5th day, and its level peaked on day 8. On day 8, PARIS formed an amorphous aggregate when incubated with 10 nM PAR (Appendix Fig S6A). Thioflavin T staining showed that solid species of PARIS underwent amorphous assembly without enhancing Thioflavin T staining, suggesting the absence of amyloid-like fibrillization (Appendix Fig S6B).

Since PARIS aggregation peaked 8 days after incubation, we checked whether PARIS triple PDM could form irreversible aggregates by day 8. PARIS triple PDM did not form aggregates in the presence or absence of 10 nM PAR (Fig 5B). The level of thioflavin T fluorescence of PARIS WT was not changed over the 8-day incubation (Appendix Fig S6C). To validate whether PAR facilitates PARIS aggregation in dopaminergic neurons, MNNG was treated to iPSC-derived human dopaminergic (hDA) neurons transduced with AAV-PARIS (Fig 5C). MNNG treatment of AAV-PARIS WT transduced hDA neurons activated PAR production and led to increased SDS-resistant high molecular weight PARIS immunoreactivity that was reduced by the PARP inhibitor, ABT-888 (Fig 5C). Taken together, these results suggest that PARIS forms high molecular weight aggregates in the presence of PAR.

To recapitulate the phase separation of PARIS observed under pathological conditions *in vivo*, we obtained the SN lysate of C57BL/N mice injected with α-syn PFFs into the striatum at postinjection 3 months and incubated them with recombinant GFP-PARIS proteins at various concentrations (0, 0.1, 0.5, 1, 3, 5, 25 μM, Appendix Fig S6D). Our observations revealed that GFP-PARIS recombinant protein underwent LLPS at a concentration of 0.1 μM, and its solidification began at the range of 0.1–0.5 μM, ultimately leading to the formation of amorphous PARIS at higher concentrations. Furthermore, we estimated the protein level of endogenous PARIS in the SN of α-syn PFF-injected mice by comparing it to recombinant PARIS reference standards (Appendix Fig S6E). Our results indicated that the PARIS level in the SN of α-syn PFF-injected

mice was approximately equivalent to 0.45 μM of recombinant PARIS, in which PARIS aggregates were observed in Appendix Fig S6D. These findings suggest that phase separation of PARIS can occur under pathological conditions *in vivo*.

Aging leads to PARIS accumulation

During the process of aging, parkin redistributes from the soluble to insoluble fraction (Pawlyk *et al*, 2003). To determine whether aging-induced reductions in parkin might lead to PARIS accumulation and aggregation, we examined the levels of parkin and its substrates, PARIS and AIMP2. Since AIMP2 can activate PARP1 (Lee *et al*, 2013), the levels of PAR were also monitored. In the SN of 7, 15, and 25 months old mice, parkin levels were reduced and PARIS, AIMP2, and PAR levels increased with age (Appendix Fig S7A and B). To examine whether the PAR-binding property of PARIS is responsible for PARIS aggregation in PAR-activating aging, PARIS WT or triple PDM was overexpressed via stereotaxic injection of Lenti-PARIS WT or PARIS triple PDM into the SN of 8-week-old C57BL/6N mice (Fig 6A). Lenti-PARIS injection led to a greater than the two-fold increase of PARIS in the SN at post-injection 1 and 20 months. High molecular weight PARIS immunoreactivity and PAR were detected in the SN of Lenti-PARIS WT-injected mice at 20 months post-injection (Fig 6A). No high molecular weight PARIS immunoreactivity was detected in Lenti-PARIS triple PDM-injected 22-month-old mice despite an increase in PAR (Fig 6A). High molecular weight PARIS immunoreactivity was not detected in the SN of Lenti-PARIS WT and PARIS triple PDM-injected mice at 1 month post-injection (Fig 6A). These results suggest that the PAR-binding property of PARIS is required to form high molecular PARIS aggregates in the presence of PAR activation.

Adult conditional knockout of parkin (cPK-KO) was performed by stereotaxic injection of AAV-GFP-Cre into the SN of 6–8-week-old *parkin*flox/flox mice (Stevens *et al*, 2015) (Fig 6B). AAV-GFP injections were used as control mice. Adult cPK-KO mice showed an

Figure 5. PAR accelerates PARIS aggregation.

A *In vitro* aggregation assay at indicated time points with 10 μM recombinant GST-cleaved PARIS protein with or without 10 nM PAR. SDS-resistant PARIS aggregate (high molecular species) was detected by PARIS antibody (bottom panel). Relative level of aggregated PARIS is on the right side, $n = 3$ independent experiments.

B *In vitro* aggregation assay using GST-PARIS WT and triple PDM in the presence or absence of 10 nM PAR at day 8. Quantification of aggregated PARIS is presented on the right side, $n = 3$ independent experiments.

C Immunoblotting of PARIS, PAR, and actin in differentiated neurons treated with AAV-PARIS, ABT-888, and MNNG. Immunoreactivity was normalized by actin. Quantification of immunoblotting is presented on the right side, $n = 3$ per group.

Data information: Statistical significance was determined by two-way ANOVA test with Tukey *post-hoc* analysis (B) or one-way ANOVA test with Tukey *post-hoc* analysis (C). Data are expressed as mean ± SEM of three biological replicates. ***$P < 0.001$.
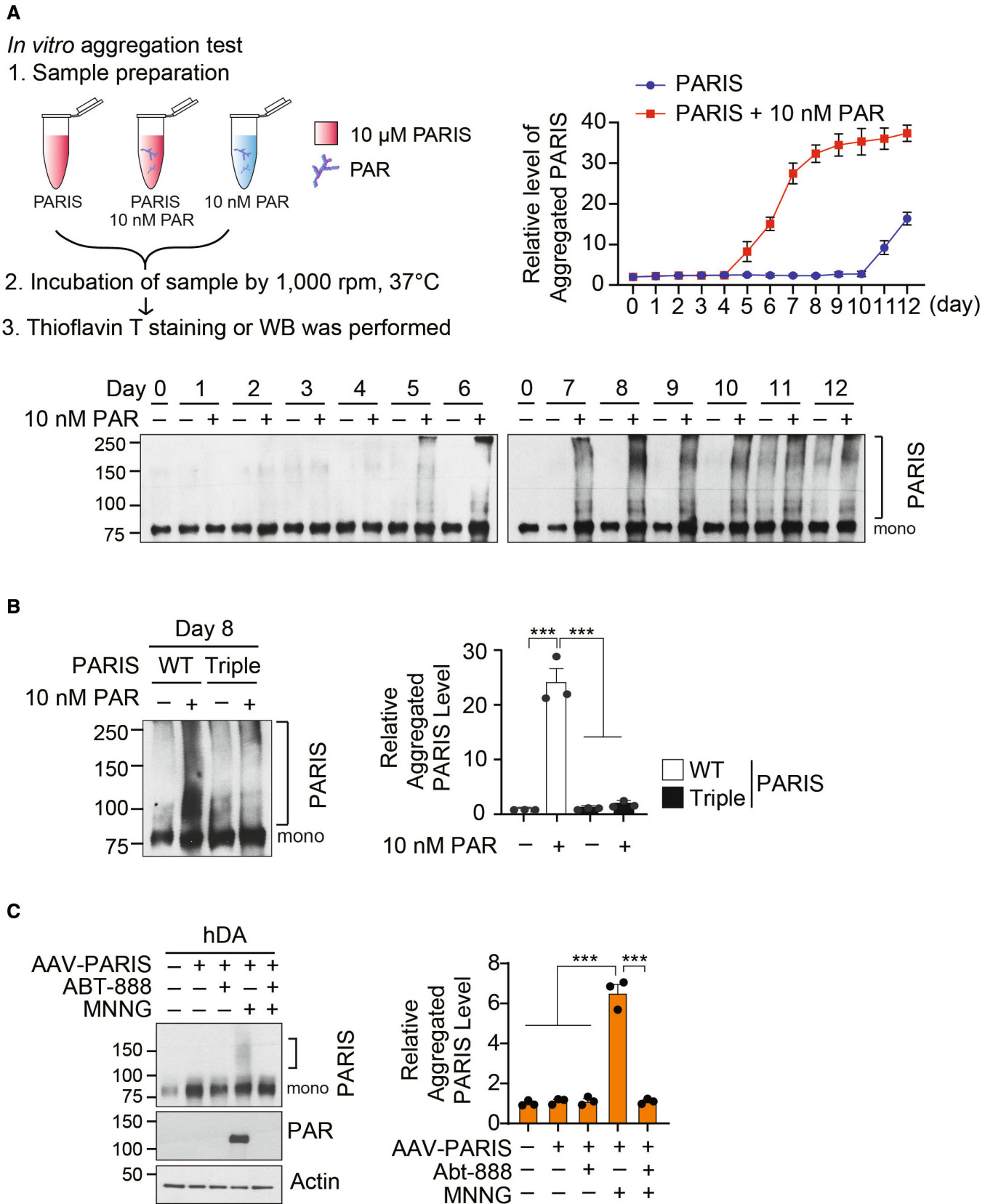
Source data are available online for this figure.

Figure 5.

accumulation of PARIS in the SN with a trend similar to that observed in the human postmortem PD brain (Shin *et al*, 2011). PARIS accumulation was found in the SN at 1- and 3-month post-injection of AAV-GFP-Cre. PAR was elevated at 3 months post-injection along with AIMP2 accumulation and the presence of SDS-resistant high molecular weight immunoreactivity of PARIS was

observed in overexposed immunoblots (Fig 6B). Next, we investigated the level of SDS-resistant PARIS in the SN of the α-synuclein preformed fibril (α-syn PFF) model of sporadic PD. PARIS and PAR levels were found to be increased in the SN at 9 months post-injection, as previously reported (Brahmachari *et al*, 2019). High molecular weight species of PARIS were observed upon
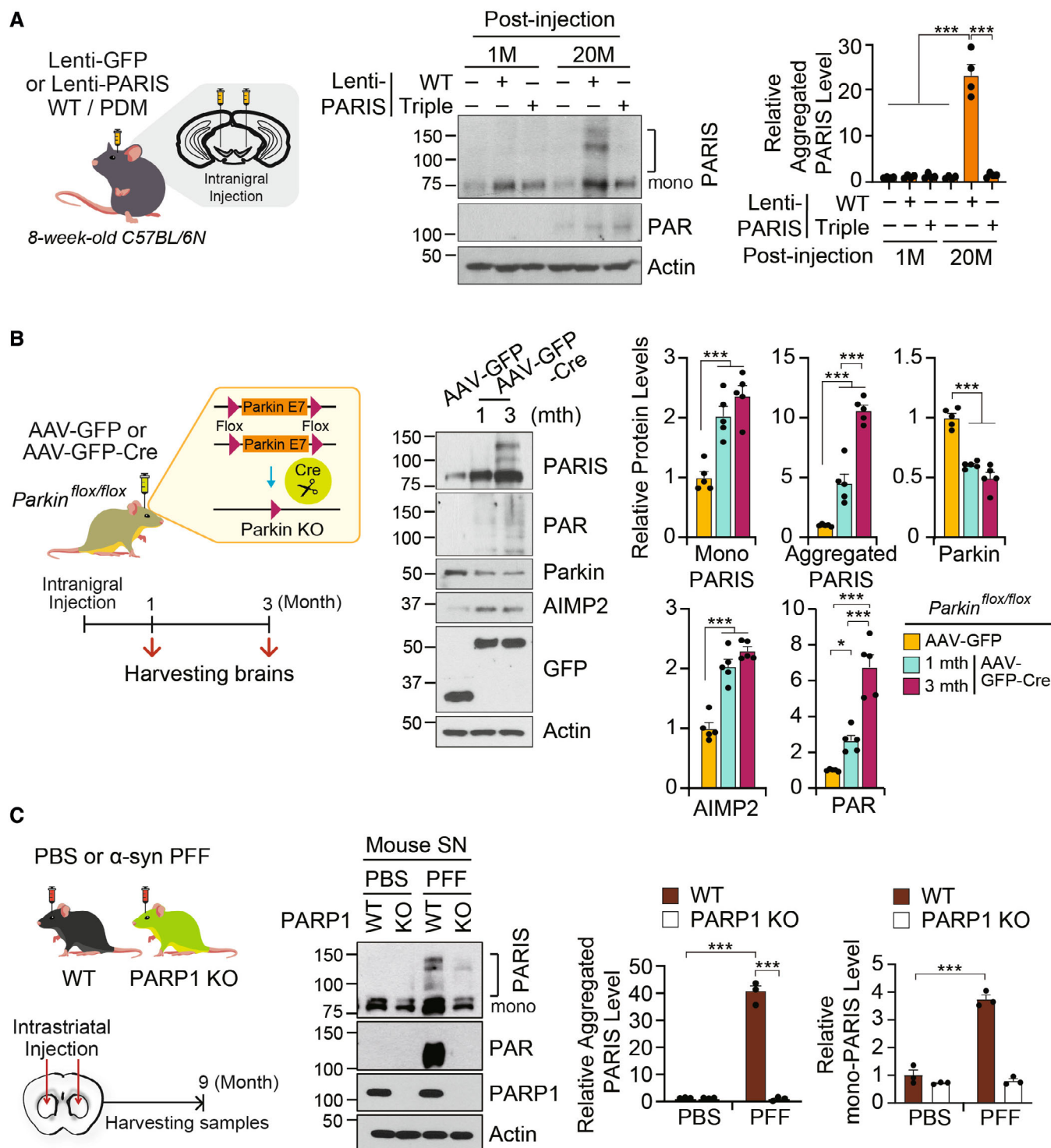

Figure 6.

Figure 6. PAR-activating stresses facilitate PARIS aggregation *in vivo*.

A   To overexpress PARIS WT or triple PDM, lentiviral vectors were stereotaxically injected into the SN of C57BL mice. At 1- and 20-month post-injection, the levels of PARIS and PAR were monitored by immunoblotting (middle panel). Relative level of PARIS aggregates was quantified on the right side. n = 4 per group.
B   Conditional parkin KO mice were generated by AAV-GFP-Cre injection into the SN of *parkin^flox/flox* mice. Representative immunoblotting of conditional parkin KO mice 1- or 3-month post-injection. Quantifications are presented at the right. n = 5 per group.
C   α-syn PFF was injected into the striatum of WT and PARP1-KO mice. At 9 months post-injection, the SN was utilized for immunoblotting analysis. Representative immunoblotting images (right panel). Relative levels of PARIS normalized to actin in the SN of α-syn PFF-injected mice. n = 3 per group.

Data information: Statistical significance was determined by two-way ANOVA test with Tukey *post-hoc* analysis (C) or one-way ANOVA test with Tukey *post-hoc* analysis (A, B). Data are expressed as mean ± SEM of biological replicates. ***$P < 0.001$.
Source data are available online for this figure.

overexposure of the immunoblots in WT mice, but not in α-syn PFF-injected PARP1-knockout (PARP1-KO) mice (Fig 6C). This demonstrates that α-syn PFF-mediated PAR activation and PARIS accumulation were cooperatively involved in PARIS solidification in the sporadic PD model (Fig 6C).

Amorphous PARIS aggregates contribute to PD pathogenesis

To investigate the relevance of PARIS phase transition to PD pathogenesis, we examined whether PAR-dependent solidification of PARIS is involved in sporadic PD animal models. We stereotaxically introduced Lenti-PARIS WT or triple PBM into the SN of PARIS knockout (KO) mice (Kim *et al*, 2021a). In addition, α-syn PFF was co-injected into the striatum of PARIS KO mice to induce a PAR-activating sporadic PD model (Fig 7A).

At 3 months postinjection, we monitored the levels of PARIS and PGC-1α in the SN, demonstrating that the PARIS aggregate was found in the SN of α-syn PFF/ Lenti-PARIS WT co-injected PARIS KO mice but not in that of α-syn PFF/Lenti-PARIS PBM co-injected PARIS KO mice (Fig 7B). As per our recent publication (Kim *et al*, 2022). PARIS aggregate is translocated to the insoluble deposit along with PGC-1α, leading to the depletion of PGC-1α in the soluble fraction. To assess whether PAR-mediated PARIS aggregation sequesters PGC-1α in α-syn PFF/Lenti-PARIS co-injected PARIS KO mice, we monitored the amount of PGC-1α in the SN of PARIS KO mice injected with α-syn PFFs ± Lenti-PARIS WT or triple PDM at postinjection 3 months (Fig 7B). As a result, the introduction of Lenti-PARIS WT and PDM caused the robust reduction of soluble PGC-1α, whereas α-syn PFF failed to change the level of PGC-1α in the SN of PARIS KO mice, suggesting that PARIS is a key player in α-syn PFF-mediated PGC-1α reduction. Moreover, we observed SDS-resistant species of PARIS in the soluble and insoluble SN lysates of α-syn PFFs/Lenti-PARIS WT-co-injected mice but not in that of α-syn PFFs/Lenti-PARIS PDM-co-injected mice, resulting in the complete loss of PGC-1α in the SN of α-syn PFFs/Lenti-PARIS WT-co-injected mice (Fig 7B).

To assess the physiological readouts by the loss of PGC-1α in α-syn PFF/Lenti-PARIS co-injected PARIS KO mice, we measured mitochondrial DNA (mtDNA) copy numbers in the SN of mice injected with α-syn PFFs ± Lenti-PARIS WT or triple PDM. The injection of Lenti-PARIS WT and PDM decreased the level of mitochondrial marker, cytochrome b (CYTB) in the SN of PBS control mice (Fig 7C). The co-administration of α-syn PFFs led to the greater reduction of mtDNA copy number in the SN of Lenti-PARIS WT-injected mice, but not in that of Lenti-PARIS PDM-injected mice (Fig 7C), indicating that PARIS's PAR-binding

property is involved in α-syn PFF-mediated mitochondrial dysregulation. In addition, we investigated whether α-syn PFF-mediated PARIS and PGC-1α aggregation contributes to DA neuronal death, showing the greater loss of DA neurons in the SN of α-syn PFFs/Lenti-PARIS WT-co-injected mice as compared to that of α-syn PFFs/Lenti-PARIS PDM-co-injected mice (Fig 7D and E). TH staining showed a significantly higher DA neuronal death in the SN of α-syn PFFs-administered mice overexpressing PARIS WT compared to overexpressing PARIS PDM (Fig 7D). These results suggest that PARIS aggregation by PAR-activating α-syn PFFs causes PGC-1α reduction and mitochondrial dysfunction, contributing to DA neuronal death in the sporadic PD model.

Discussion

The mechanism of how parkin functions through PARIS and PGC-1α to cause PD is complex and poorly understood. However, our investigations have shown that parkin promotes proteasomal degradation of PARIS, preventing PARIS from binding to the promoter of PGC-1α. The inactivation of parkin leads to PARIS accumulation and PGC-1α suppression, contributing to mitochondrial dysfunction and dopaminergic neuronal death (Shin *et al*, 2011; Stevens *et al*, 2015).

Recent research has shown that exposure to α-syn PFF can activate the non-receptor tyrosine kinase c-Abl, in turn, leads to parkin phosphorylation and inactivation, and PARIS accumulation (Brahmachari *et al*, 2019). We also found that c-Abl directly phosphorylates PARIS at Y137 and drives its interaction with KAP1, a transcriptional repressor, leading to p53-dependent cell death (Kim *et al*, 2021b). In addition, PINK1 interacts with and phosphorylates PARIS, and subsequently, parkin ubiquitinates phosphorylated PARIS, alleviating PARIS-mediated PGC-1α repression and toxicity (Lee *et al*, 2017). Similar to parkin inactivation, the loss of PINK1 results in PARIS accumulation (Lee *et al*, 2017). The administration of MPTP (1-methyl-4-phenyl-1,2,3,6-tetrahydropyridine) can also elevate PARIS amount (Rudenok *et al*, 2020; Kim *et al*, 2022).

Overall, PD-associated molecular changes such as α-syn PFF formation, c-Abl activation, parkin-pink1 inactivation, and MPTP-mediated mitochondrial damages can contribute to the elevation of PARIS. Therefore, understanding the mechanisms underlying the physiological and pathological function of PARIS in dopaminergic neurons can be important for developing effective treatments for PD.

In this study, we demonstrated that PARIS undergoes LLPS and liquid–solid transition via PARIS self-assembly. In the step of PD pathogenesis, various PD causative factors lead to the accumulation of PARIS, resulting in an imbalance of energy metabolism and PAR
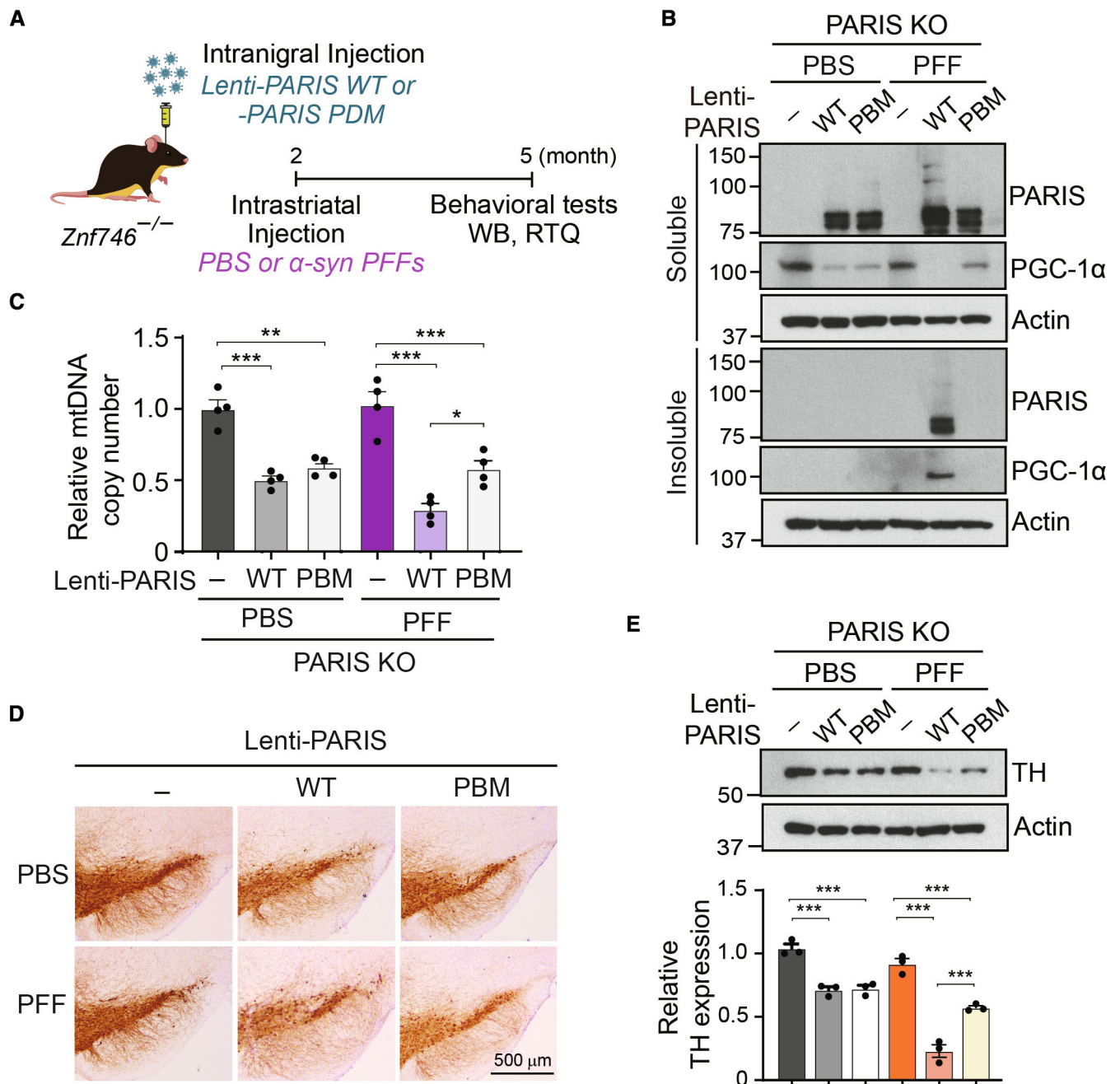
Figure 7. PAR-mediated PARIS aggregation contributes to PD pathogenesis.

A   Lenti-PARIS WT or triple PDM were stereotaxically injected into the SN of PARIS KO mice. α-syn PFF was injected into the striatum of PARIS KO mice at 2 months of age.

B   At post-injection 6 months, the levels of PARIS and PGC-1α were measured in the soluble and insoluble fraction of SN region using immunoblot analysis.

C   Measurement of the relative level of cytochrome b (CYTB) normalized to GAPDH level. *n* = 4.

D   Representative TH-stained images of the midbrain sections from injected, Scale bar = 500 μm.

E   Relative TH expression was evaluated using immunoblot analysis, *n* = 3.

Data information: Statistical significance was determined by a one-way ANOVA test with Tukey *post-hoc* analysis (C, E). Data are expressed as mean ± SEM of biological replicates. *$P < 0.05$, **$P < 0.01$, and ***$P < 0.001$.

Source data are available online for this figure.

overactivation. PAR polymers attach to PARIS and enhance self-assembly, forming insoluble species that sequester PGC-1α in aggregate deposit.

The protein sequence of PARIS bears 10 IDRs, including five LCDs as well as the prion-like sequence at LCD4. Recombinant PARIS (10 μM) formed liquid droplets under physiological

conditions without the use of a crowding agent (Fig 1B). Since FUS and TDP-43, causative factors of ALS, form liquid droplets at 10 μM protein concentration only in the presence of crowding agents, PARIS might possess a much stronger propensity to undergo phase separation as compared to FUS and TDP-43. In addition, it was recently discovered that the LCD and PrLD of FUS mediate LLPS. A solid transition of FUS is enhanced by proline or serine insertion between poly-glycine sequences (Wang *et al*, 2018). Similarly, we identified that PARIS LLPS was dependent upon its LCD1, and the PrLD of PARIS was required for amorphous aggregation (Fig 3C). Since the prion-like sequence of PARIS contains glycine and serine residues, we speculate that the combination of unique residues contributes to its solidification.

Poly(ADP-ribose) is known to seed liquid demixing of intrinsically disordered proteins such as FUS, EWS, and TAF15. In a PD model, treatment with α-syn PFF activates PAR production, and PAR converts α-synuclein to a more toxic strain, contributing to neurodegeneration. Moreover, PAR binds to and triggers TDP-43 assembly and the inhibition of tankyrase prevents cytoplasmic accumulation of TDP-43 and neuronal death. In this study, we found that PARIS binds PAR, and 10 nM PAR accelerates PARIS aggregation at 25 μM protein concentration (Fig 4A and B). PAR formation appears to cause SDS-resistant PARIS aggregates in mice. Consistent with this notion is our observation that lentivirus-mediated PARIS overexpression led to the formation of SDS-resistant PARIS immunoreactivity in the setting of elevated PAR (Fig 6A). Moreover, in the SN of adult cPK-KO mice, SDS-resistant PARIS immunoreactivity was also observed in the setting of elevated PAR. α-syn PFF striatal injection upregulated the levels of both PARIS and PAR (Kam *et al*, 2018; Brahmachari *et al*, 2019), leading to high molecular weight species of PARIS that were prevented by knockout of PARP1 suggesting that PAR may lead to solidification of PARIS *in vivo* (Fig 6).

In summary, PARIS undergoes LLPS and liquid to solid transition, contributing to the formation of amorphous solid aggregates. LCD1 is required for the liquid assembly of PARIS and the prion-like sequence is critical for PARIS aggregation. Furthermore, PAR binds to PARIS and promotes PARIS aggregation. What role PARIS LLPS plays in the physiological function of PARIS and whether PAR promotion of PARIS aggregation contributes to neurodegeneration requires further study.

Materials and Methods

Antibodies

The list of antibodies used in this study is indicated in Appendix Table S1.

DNA construction and mutagenesis

pGEX6p1-PARIS, GFP-PARIS, and Flag-PARIS constructs have been described previously (Shin *et al*, 2011). pCR8/GW-ZNF746 vector was used to perform PARIS LC domain deletion and PAR binding point mutation. For domain deletion and point mutation, the Agilent Quick Change II XL kit was used according to the manufacturer's protocol. DNA constructs were verified via sequencing. PARIS truncation constructs were cloned into pCR8/GW vector using pCR8/GW/TOPO kit (Invitrogen) and subcloned into pcDNA6.2emGFP and pDEST15 (Thermo) through Gateway cloning by LR clonase (Invitrogen). Primer sequences are described in Appendix Table S2.

Bioinformatic prediction for protein domain, disorder, and charge

The full-length ZNF746 sequence was obtained from PubMed (ZNF746, NP_689770.3). The protein domain of human PARIS (ZNF746) was analyzed by Pfam (https://pfam.xfam.org/). Protein disorder was predicted by PONDR (http://www.pondr.com/). Prion-like sequence prediction was performed by PLAAC (http://plaac.wi.mit.edu/). Amino acid classification of PARIS was performed based on the charge state of amino acids.

Purification of recombinant PARIS protein

pGEX6p1 PARIS WT and mutant (ΔLCD mutants, Truncation, Triple, Δ7, and ΔPrLD) constructs were transformed to BL21 gold (Agilent). BL21 *E. coli* was grown at 37°C. When optical density reached 0.6–0.8, the culture was chilled using ice for 1 h. 1 mM IPTG was used to induce protein expression. *E. coli* was incubated at 16°C overnight and was spun down at 3,000 × *g* for 20 min at 4°C. CelLytic B reagent (Sigma) was used to lyse *E. coli* cells, according to the manufacturer's protocol. Glutathione sepharose (GE HealthCare) was used to pull down the proteins for 3 h at 4°C. For GST-PARIS purification, protein-bound beads were eluted in elution buffer for 1 h at 4°C (50 mM HEPES, pH 7.5, 100 mM NaCl, 30% glycerol, 40 mM reduced glutathione, and 0.03% Triton X-100). To remove GST, PreScission protease (GE HealthCare) was used as a manufacturer's protocols. Recombinant proteins were concentrated by Amicon Ultra-15 (30K and 100K) filter. After purification, proteins were submitted for SDS–PAGE.

In vitro LLPS assay

To perform LLPS assay, purified WT or mutant PARIS were mixed with 150 or 500 mM NaCl and incubated for 2 h at room temperature (RT). After incubation, 5 μl of each sample was applied on a microscope slide (Thermo) and covered with 12 mm coverslips (Fisherbrand). PEG and 1,6-hexanediol (Sigma) were added to the sample as indicated. PAR was purchased from Trevigen. Images were taken under a Leica microscope (CTR 6000).

FRAP

For *in vitro* FRAP experiment, 10 or 50 μM PARIS in 150 mM NaCl was incubated for 2 h. Thereafter, 5 μl of each sample was applied to 22 × 50 mm coverslips and sandwiched with 12 mm coverslips (Fisherbrand). To perform photobleaching, a laser scanning confocal microscope (Zeiss, LSM 710) was used with 100% laser power with 200 iterations. Fluorescence intensity of the region of interest (ROI1) was normalized through the values of total intensity (ROI2) and background intensity (ROI3) of the subject. The fluorescence recovery curve was calculated using easyFRAP (https://easyfrap.vmnet.upatras.gr), and $t_{1/2}$ was analyzed by FRAPbot (http://frapbot.kohze.com/).

TEM

Transmission electron microscopy was performed with a Zeiss Sigma 500 with a TEM detector at 25 kV. A total of 20 μl of the sample was spotted on a parafilm-covered glass slide and covered with a formvar/carbon grid (Ted Pella) for 5 min. After two washes with distilled water, the grid with the sample was stained with 1% (w/v) uranyl formate for 1 min and air-dried.

Circular dichroism spectroscopy

Ten microliters of the aged PARIS protein sample were diluted with 190 μl of 150 mM NaCl solution. Samples were measured between 260 and 200 nm with 100 nm/min speed at RT. Buffer subtraction and smoothing proceeded.

Cell culture and transfection

SH-SY5Y cells (ATCC) were cultured at 37°C with 5% CO_2 and fed with DMEM supplemented with 10% FBS and 1% antibiotic-antimycotic (v/v). Cells were trypsinized with 0.25% trypsin and plated. The next day, the indicated drugs or plasmids were administered. PARP1-KO SH-SY5Y cell lines were generated by the CRISPR/Cas9 system.

Immunoprecipitation

SH-SH5Y cells were plated in a 6-well plate and transfected with the indicated plasmids. After 48 h, cells were washed twice with ice-cold phosphate-buffered saline (PBS), and centrifuged at $1,000 \times g$ at 4°C for 5 min. Cells were lysed with RIPA buffer (Thermo) with protease inhibitor (G bioscience). The lysate was frozen and thawed three times. Lysates were centrifuged at $13,000 \times g$ for 30 min at 4°C. Supernatants were mixed with equilibrated Protein G Sepharose beads (GE HealthCare) and indicated antibody. Mixtures were incubated overnight at 4°C. Collected beads were washed three times with ice-cold RIPA buffer and boiled with 2× SDS sample buffer (Bio-Rad) for 10 min at 95°C.

Protein modeling

The structure of PARIS TM#1 was predicted via COTH analysis by the Zhang lab (https://zhanglab.ccmb.med.uMich.edu/COTH), and LC 1 region dimer formation was modeled by PREDDIMER (https://preddimer.nmr.ru/).

PAR overlay

Recombinant PARIS proteins or cell lysates were transferred to an NC membrane by dot blotting (Bio-Dot SF, Bio-Rad) or SDS–PAGE. The NC membranes were incubated with 5 nM PAR (Trevigen) in PBS with 0.5% Tween-20 (PBS-T) for 2 h at RT. After incubation, the membranes were washed three times with PBS-T for 10 min each. The membranes were then blocked with 5% skimmed milk in PBS-T for 30 min and incubated with the PAR antibody at a 1:3,000 ratio (Trevigen) for 2 h at RT. The membranes were washed three times with PBS-T for 10 min each and incubated with the anti-rabbit secondary antibody at a

1:5,000 ratio for 30 min at RT. PAR binding was detected using the chemiluminescent ECL reagent (Thermo).

iPS-derived hDA neuron culture

For the differentiation of hDA neurons, H1 hESCs were used. H1 cells were first plated as single cells in high density in Matrigel-coated plates. After treatment with dopamine neuron-specific factors for 11 days, these stem cells developed into neural precursor cells (NPCs). NPCs were then re-plated on poly-D-lysine & laminin-coated plates and fed every day with neurobasal media until maturation (approximately 60 days after NPC re-plating) (Yun *et al*, 2018).

In vitro aggregation assay

Ten micromole PARIS protein was mixed with various concentrations of PAR. To minimize the effects of light exposure and prevent evaporation, samples were incubated in a small opaque container with a secure lid at 37°C at 1,000 rpm, and samples were collected daily. After day 8, samples were loaded to SDS–PAGE and detected with the PARIS antibody.

Thioflavin T staining

Fibrillization of PARIS was measured via thioflavin T staining. Samples from the aggregation assay were collected and mixed with 25 μM thioflavin T solution in PBS. After 10 min incubation, fluorescence was measured using Agilent microplate multiscanner (Agilent) (excitation: 450 nm, emission: 510 nm).

PCR analysis for mtDNA copy number

Total DNA was extracted with the QIAzol lysis reagent (Qiagen, Hilden, Germany). Relative quantities of mtDNA were analyzed using the Rotor-Gene Q real-time PCR (Qiagen, Hilden, Germany) and Rotor-Gene SYBR green PCR kit (Qiagen, Hilden, Germany), according to the manufacturer's instructions. The primer sequences are listed in the Appendix Table S2.

Animal experiments

Mouse experiments followed the guidelines of the Association for Assessment and Accreditation of Laboratory Animal Care guidelines under the supervision of Sungkyunkwan University Institutional Animal Care and Use Committee (IACUC, SKKUIACUC2022-07-42-1). C57BL/6N mice were purchased (Orient) and maintained under a 12/12 h (h) dark/light cycle in air-controlled rooms, with access to diet and water for the experiments.

Stereotaxic injection

Lentiviruses overexpressing PARIS WT and PBM (Lenti-PARIS WT and PBM) were made as previously described (Caiazzo *et al*, 2011). Briefly, 8-week-old C57BL/6N mice were used for the experiment. Mice were anesthetized with isoflurane. Coordination of SN was as follows: anteroposterior, 3.0 mm from bregma; mediolateral, 1.2 mm; dorsoventral, 4.3 mm. AAV-GFP and AAV-GFP-Cre were

purchased from Iowa University and utilized for *parkin*^*flox/flox* mice as previously described (Stevens *et al*, 2015).

α-syn PFF preparation

Recombinant α-synuclein was purified, and α-syn PFF was generated as described previously (Kam *et al*, 2018), followed by the removal of bacterial endotoxins (ToxinEraser Endotoxin Removal Kit, GeneScript).

Stereotaxic injection of α-syn PFF

α-syn PFF was injected into 3-month-old PARP1 WT and KO mice (Jackson Laboratory, #002779) as previously described (Kam *et al*, 2018). Mice were anesthetized with isoflurane. PBS or 5 μg of α-syn PFF was injected unilaterally into the striatum. The coordination of the striatum was as follows: anteroposterior, 0.2 mm from bregma; mediolateral, 2 mm; dorsoventral, 2.8 mm.

Mouse brain sample preparation

The SN region of mouse brain was dissected by brain block (Roboz). RIPA buffer supplemented with protease inhibitor was added to tissues. Tissues were homogenized by 1 ml homogenizer (Wheaton) 10 times and then were frozen and thawed three times. To obtain total cell lysate, samples were boiled with 2× SDS sample buffer for 10 min at 95°C.

Statistical analysis

Student's *t*-test was used to compare the two groups. One-way and two-way ANOVA tests were used to compare multiple samples followed by Tukey's *post-hoc* analysis (GraphPad 8.0.2).

Data availability

This study includes no data deposit in external repositories.

Expanded View for this article is available online.

Author contributions

Hojin Kang: Conceptualization; data curation; validation; investigation; visualization; methodology; writing – original draft. **Soojeong Park:** Data curation; validation; investigation; visualization; methodology; writing – review and editing. **Areum Jo:** Conceptualization; data curation; investigation; methodology. **Xiaobo Mao:** Resources; formal analysis. **Manoj Kumar:** Resources; software; formal analysis. **Chi-Hu Park:** Resources; software; formal analysis. **Jee-Yin Ahn:** Resources; supervision; methodology. **Yunjong Lee:** Resources; supervision; methodology. **Jeong-Yun Choi:** Resources; supervision; methodology. **Yun-Song Lee:** Resources; supervision; methodology. **Valina L Dawson:** Resources; methodology; writing – review and editing. **Ted M Dawson:** Resources; methodology; writing – review and editing. **Tae-In Kam:** Conceptualization; resources; supervision; writing – original draft; project administration; writing – review and editing. **Joo-Ho Shin:** Conceptualization; resources; supervision; funding acquisition; visualization; writing – original draft; project administration; writing – review and editing.

Disclosure and competing interests statement
The authors declare that they have no conflict of interest.

References

Ahel I, Ahel D, Matsusaka T, Clark AJ, Pines J, Boulton SJ, West SC (2008) Poly (ADP-ribose)-binding zinc finger motifs in DNA repair/checkpoint proteins. *Nature* 451: 81–85

Alberti S, Dormann D (2019) Liquid-liquid phase separation in disease. *Annu Rev Genet* 53: 171–194

Altmeyer M, Neelsen KJ, Teloni F, Pozdnyakova I, Pellegrino S, Grofte M, Rask MD, Streicher W, Jungmichel S, Nielsen ML *et al* (2015) Liquid demixing of intrinsically disordered proteins is seeded by poly(ADP-ribose). *Nat Commun* 6: 8088

Baradaran-Heravi Y, Van Broeckhoven C, van der Zee J (2020) Stress granule mediated protein aggregation and underlying gene defects in the FTD-ALS spectrum. *Neurobiol Dis* 134: 104639

Berger NA, Besson VC, Boulares AH, Burkle A, Chiarugi A, Clark RS, Curtin NJ, Cuzzocrea S, Dawson TM, Dawson VL *et al* (2018) Opportunities for the repurposing of PARP inhibitors for the therapy of non-oncological diseases. *Br J Pharmacol* 175: 192–222

Brahmachari S, Lee S, Kim S, Yuan C, Karuppagounder SS, Ge P, Shi R, Kim EJ, Liu A, Kim D *et al* (2019) Parkin interacting substrate zinc finger protein 746 is a pathological mediator in Parkinson's disease. *Brain* 142: 2380–2401

Caiazzo M, Dell'Anno MT, Dvoretskova E, Lazarevic D, Taverna S, Leo D, Sotnikova TD, Menegon A, Roncaglia P, Colciago G *et al* (2011) Direct generation of functional dopaminergic neurons from mouse and human fibroblasts. *Nature* 476: 224–227

Dawson TM, Dawson VL (2017) Mitochondrial mechanisms of neuronal cell death: potential therapeutics. *Annu Rev Pharmacol Toxicol* 57: 437–454

Franzmann TM, Alberti S (2019) Prion-like low-complexity sequences: key regulators of protein solubility and phase behavior. *J Biol Chem* 294: 7128–7136

Gagne JP, Isabelle M, Lo KS, Bourassa S, Hendzel MJ, Dawson VL, Dawson TM, Poirier GG (2008) Proteome-wide identification of poly(ADP-ribose) binding proteins and poly(ADP-ribose)-associated protein complexes. *Nucleic Acids Res* 36: 6959–6976

Harrison AF, Shorter J (2017) RNA-binding proteins with prion-like domains in health and disease. *Biochem J* 474: 1417–1438

Kam TI, Mao X, Park H, Chou SC, Karuppagounder SS, Umanah GE, Yun SP, Brahmachari S, Panicker N, Chen R *et al* (2018) Poly(ADP-ribose) drives pathologic alpha-synuclein neurodegeneration in Parkinson's disease. *Science* 362: eaat8407

Kang H, Shin JH (2015) Repression of rRNA transcription by PARIS contributes to Parkinson's disease. *Neurobiol Dis* 73: 220−228

Kang H, Jo A, Kim H, Khang R, Lee JY, Kim H, Park CH, Choi JY, Lee Y, Shin JH (2018) PARIS reprograms glucose metabolism by HIF-1alpha induction in dopaminergic neurodegeneration. *Biochem Biophys Res Commun* 495: 2498−2504

Kim H, Kang H, Lee Y, Park CH, Jo A, Khang R, Shin JH (2017) Identification of transketolase as a target of PARIS in substantia nigra. *Biochem Biophys Res Commun* 493: 1050−1056

Kim H, Lee JY, Park SJ, Kwag E, Koo O, Shin JH (2021a) ZNF746/PARIS promotes the occurrence of hepatocellular carcinoma. *Biochem Biophys Res Commun* 563: 98−104

Kim H, Shin JY, Jo A, Kim JH, Park S, Choi JY, Kang HC, Dawson VL, Dawson TM, Shin JH *et al* (2021b) Parkin interacting substrate phosphorylation by c-Abl drives dopaminergic neurodegeneration. *Brain* 144: 3674−3691

Kim H, Lee JY, Park SJ, Kwag E, Kim J, Shin JH (2022) S-nitrosylated PARIS leads to the sequestration of PGC-1alpha into insoluble deposits in Parkinson's disease model. *Cell* 11: 3682

Krietsch J, Rouleau M, Pic E, Ethier C, Dawson TM, Dawson VL, Masson JY, Poirier GG, Gagne JP (2013) Reprogramming cellular events by poly(ADP-ribose)-binding proteins. *Mol Aspects Med* 34: 1066−1087

Lee Y, Karuppagounder SS, Shin JH, Lee YI, Ko HS, Swing D, Jiang H, Kang SU, Lee BD, Kang HC *et al* (2013) Parthanatos mediates AIMP2-activated age-dependent dopaminergic neuronal loss. *Nat Neurosci* 16: 1392−1400

Lee Y, Stevens DA, Kang SU, Jiang H, Lee YI, Ko HS, Scarffe LA, Umanah GE, Kang H, Ham S *et al* (2017) PINK1 primes parkin-mediated ubiquitination of PARIS in dopaminergic neuronal survival. *Cell Rep* 18: 918−932

Leung AKL (2020) Poly(ADP-ribose): a dynamic trigger for biomolecular condensate formation. *Trends Cell Biol* 30: 370−383

McAlary L, Plotkin SS, Yerbury JJ, Cashman NR (2019) Prion-like propagation of protein misfolding and aggregation in amyotrophic lateral sclerosis. *Front Mol Neurosci* 12: 262

McGurk L, Gomes E, Guo L, Mojsilovic-Petrovic J, Tran V, Kalb RG, Shorter J, Bonini NM (2018) Poly(ADP-ribose) prevents pathological phase separation of TDP-43 by promoting liquid demixing and stress granule localization. *Mol Cell* 71: 703−717

Nott TJ, Petsalaki E, Farber P, Jervis D, Fussner E, Plochowietz A, Craggs TD, Bazett-Jones DP, Pawson T, Forman-Kay JD *et al* (2015) Phase transition of a disordered nuage protein generates environmentally responsive membraneless organelles. *Mol Cell* 57: 936−947

Patel A, Lee HO, Jawerth L, Maharana S, Jahnel M, Hein MY, Stoynov S, Mahamid J, Saha S, Franzmann TM *et al* (2015) A liquid-to-solid phase transition of the ALS protein FUS accelerated by disease mutation. *Cell* 162: 1066−1077

Pawlyk AC, Giasson BI, Sampathu DM, Perez FA, Lim KL, Dawson VL, Dawson TM, Palmiter RD, Trojanowski JQ, Lee VM (2003) Novel monoclonal antibodies demonstrate biochemical variation of brain parkin with age. *J Biol Chem* 278: 48120−48128

Peskett TR, Rau F, O'Driscoll J, Patani R, Lowe AR, Saibil HR (2018) A liquid to solid phase transition underlying pathological huntingtin Exon1 aggregation. *Mol Cell* 70: 588−601

Ray S, Singh N, Kumar R, Patel K, Pandey S, Datta D, Mahato J, Panigrahi R, Navalkar A, Mehra S *et al* (2020) alpha-Synuclein aggregation nucleates through liquid-liquid phase separation. *Nat Chem* 12: 705−716

Rudenok MM, Alieva AK, Starovatykh JS, Nesterov MS, Stanishevskaya VA, Kolacheva AA, Ugryumov MV, Slominsky PA, Shadrina MI (2020) Expression analysis of genes involved in mitochondrial biogenesis in mice with MPTP-induced model of Parkinson's disease. *Mol Genet Metab Rep* 23: 100584

Shin Y, Brangwynne CP (2017) Liquid phase condensation in cell physiology and disease. *Science* 357: eaaf4382

Shin JH, Ko HS, Kang H, Lee Y, Lee YI, Pletinkova O, Troconso JC, Dawson VL, Dawson TM (2011) PARIS (ZNF746) repression of PGC-1alpha contributes to neurodegeneration in Parkinson's disease. *Cell* 144: 689−702

Stevens DA, Lee Y, Kang HC, Lee BD, Lee YI, Bower A, Jiang H, Kang SU, Andrabi SA, Dawson VL *et al* (2015) Parkin loss leads to PARIS-dependent declines in mitochondrial mass and respiration. *Proc Natl Acad Sci USA* 112: 11696−11701

Toretsky JA, Wright PE (2014) Assemblages: functional units formed by cellular phase separation. *J Cell Biol* 206: 579−588

Wang J, Choi JM, Holehouse AS, Lee HO, Zhang X, Jahnel M, Maharana S, Lemaitre R, Pozniakovsky A, Drechsel D *et al* (2018) A molecular grammar governing the driving forces for phase separation of prion-like RNA binding proteins. *Cell* 174: 688−699

Wegmann S, Eftekharzadeh B, Tepper K, Zoltowska KM, Bennett RE, Dujardin S, Laskowski PR, MacKenzie D, Kamath T, Commins C *et al* (2018) Tau protein liquid-liquid phase separation can initiate tau aggregation. *EMBO J* 37: e98049

Wei Y, Thyparambil AA, Latour RA (2014) Protein helical structure determination using CD spectroscopy for solutions with strong background absorbance from 190 to 230nm. *Biochim Biophys Acta* 1844: 2331−2337

Yun SP, Kam TI, Panicker N, Kim S, Oh Y, Park JS, Kwon SH, Park YJ, Karuppagounder SS, Park H *et al* (2018) Block of A1 astrocyte conversion by microglia is neuroprotective in models of Parkinson's disease. *Nat Med* 24: 931−938